Title
Deposition and Characterization of Post-growth annealed ZnSnN2 thin films.

Author
Korlam, Sudheer

Publication Date
2017

Peer reviewed|Thesis/dissertation

UNIVERSITY OF CALIFORNIA

Los Angeles

Deposition and Characterization of Post-growth annealed $ZnSnN_2$ thin films.

A thesis submitted in partial satisfaction

of the requirements for the degree Master of Science

in Materials Science and Engineering

by

Sudheer Korlam

2017

ABSTRACT OF THE THESIS

Deposition and Characterization of Post-growth annealed ZnSnN2 thin films.

by

Sudheer Korlam

Master of Science in Materials Science and Engineering

University of California, Los Angeles, 2017

Professor Dwight Christopher Streit, Chair

In order to cater to modern day photovoltaic and solar needs, semiconductor materials which are earth abundant with a direct bandgap (E_g) around 1.5eV are necessary[1,2] . Of the commonly known semiconductor materials like Si, Ge or binary III-V (Where III = B, A, Ga, In and V = N, P, As, Sb) and II-VI (Where II = Zn, Cd; and VI = O, S, Se, Te), only a few candidates consist of bandgaps which are in the range 1.0–2.0 eV. The requirement for efficient, high quality photovoltaics energy conversion and opto-electronic devices which can be an alternative to the current available semiconductor materials inspires the search for other earth abundant materials [3]. One way to search for these new materials is by studying ternary or multi-ternary semiconductor materials which have more opto-electronic properties.

The Zn-IV-N_2 group of semiconductor materials has been attracting a lot of attention following the synthesis of Sn containing material, $ZnSnN_2$[4-5]. These novel Zn-IV-N_2 group of semiconductor materials can act as a potential earth abundant alternative to InGaN and other thin

film solar cell materials such as CdTe and $CuInGaSe_2$ for use in light generation and light absorption applications. For materials such as $Zn(Ge,Sn)N_2$ alloys, absorption edges which are in the range of 2.0 – 3.1eV have been shown already[6]. And an even larger spectral distribution from the infrared region to the ultraviolet region is expected for $Zn(Si,Sn)N_2$ alloys. Even wider spectral coverage from the infrared to the ultraviolet is predicted for $Zn(Si,Sn)N_2$ alloys[7]. Of all the potential options, the $ZnSnN_2$ material exhibits properties such as large optical absorption coefficient and a tunable bandgap range among others that make it a really good potential material as the absorber layer for the next generation PV devices.

One of the major challenges facing this material is the discrepancies between the measured and calculated bandgap values. The calculated bandgap values are in the range of 0.35 – 2.64 eV depending on the crystal structure assumed[39] . Whereas the value of the experimental bandgap lies between 1.7 -2.1 eV [40]. One of the reasons for this inability to converge on a bandgap value has been attributed to the bandgap filling due to the degenerate carrier concentration of the material[38] (around 10^{21} – 10^{22} per cm^{-3}).

In this dissertation, issues related to the carrier concentration in $ZnSnN_2$ material are studied. Most of the work done focuses on efforts to reduce the carrier concentration in $ZnSnN_2$ films to around 10^{18} per cm^{-3} range. The growth method used for growing the $ZnSnN_2$ films was RF sputtering using Zn-Sn cathodes containing Zn-Sn in the ratio 3:1. RF Sputtering was chosen because it produces films that are more uniform than the films fabricated using other methods like vapor-liquid-solid plasma assisted growth or CVD[41]. The films were grown on c-plane Sapphire and (0001) GaN substrates. The so obtained films were characterized using X-ray diffraction (XRD), Scanning electron microscopy (SEM) and Hall Effect measurement.

The films were later subjected to rapid thermal annealing (RTA) at various temperatures to study the effect of rapidly heating the samples to high temperatures, holding them for a given time and cooling them quickly. The samples subjected to RTA were characterized by XRD, SEM and Hall Effect measurements. The results indicated a significance decrease in the electron concentration of the material after the annealing process which could make $ZnSnN_2$ an interesting alternative as an earth abundant semiconductor material for future absorber layers.

The thesis of Sudheer Korlam is approved.

Ya-Hong Xie

Mark S. Goorsky

Dwight Christopher Streit, Chair

University of California, Los Angeles

2017

Table of Contents –

1. Introduction

1.1 Motivation …… 1

1.2 Objective……... 2

2. Background

2.1 Zn-IV-N_2 Group …….. 3

2.2 Synthesis methods ……... 7

3. Experimental Section

3.1 Materials used……. 12

3.2 Substrate cleaning……... 12

3.3 Distinguishing between GaN and Sapphire surfaces…….. 14

3.4 Deposition of $ZnSnN_2$ thin films…… 15

3.5 Rapid Thermal Annealing treatment……... 16

4. Characterization of $ZnSnN_2$ films

4.1 High resolution X-ray diffraction……... 17

4.2 Surface Morphology……... 24

4.3 Electrical Properties…… 27

5. Conclusion…… 36

References…… 38

List of Figures

Fig. 2.1- The relative abundance of elements in the Earth's upper continental crust in terms of the US Geology Survey……. 3

Fig. 2.2 - Crystal structures of GaN and Zn-IV-N2 compounds. (a) A 3D view of GaN crystal structure: the small light grey spheres are N atoms and the large yellow spheres are Ga atoms. (b) A 3D view of Zn-IV-N2 crystal structure: the small red spheres are N atoms, the light green spheres are group IV atoms (Si, Sn or Ge) and the dark blue spheres are Zn atoms. (c) The wurtzite GaN and orthorhombic ZnSnN2 oriented along the (0001) direction……. 4

Fig. 2.3 - Band gaps versus lattice constants "a" in III-N and Zn-IV-N2 nitrides……... 10

Fig 3.1 – Schematic for the procedure used in Stage 1 of cleaning…….. 11

Fig 3.2- Schematic for the procedure used in Stage 2 of cleaning……... 11

Fig 3.3 – Contact angles of water drops on the GaN and Sapphire sides of the substrate…… 13

Fig 3.4– Cross-section figure of the deposited ZnSnN2 film and the substrate……... 14

Fig 4.1 – Calculated XRD pattern for the deposited ZnSnN2 films……. 17

Fig 4.2– Measured XRD patterns for a) Sample wit as deposited ZnSnN2 film b) Samples subjected to RTA at 350^{o}C. c) Samples subjected to RTA at 400^{o}C d) Samples subjected to RTA at 450^{o}C e) Samples subjected to RTA at 500^{o}C f) samples subjected to vacuum anneal at 400^{o}C……. 20

Fig 4.3– Background stripped XRD patterns of the samples subjected to RTA at various temperatures…….. 20

Fig 4.4 - 2θ – ω vs Intensity for ZnSnN2 samples annealed a different conditions…….. 22

Fig 4.5- SEM image of ZnSnN2 thin films deposited at the substrate temperature of 400 ˚C and vacuum annealed for 4 hours with N2/(N2+Ar) ratio of 50%. (SEM conditions are HV=10kV, WD=5.3 mm, spot size=3.0, and scale bar=1um)……. 23

Fig 4.6- SEM image of ZnSnN2 thin films deposited at the substrate temperature of 400 ˚C and vacuum annealed for 4 hours with N2/(N2+Ar) ratio of 50%. (SEM conditions are HV=10kV, WD=5.3 mm, spot size=3.0, and scale bar=500nm and 200nm)……..... 24

Fig 4.7 - SEM image of ZnSnN2 thin films deposited at the substrate temperature of 400 ˚C and rapid thermal annealed at 450oC with N2/(N2+Ar) ratio of 50%. (SEM conditions are HV=10kV and 5kV, WD=5.3 mm, spot size=2.0 and 3.0, and scale bar=1um)…….. 24

Fig 4.8 – Graph for the carrier concentration in the ZnSnN2 films annealed at different temperatures for 20 min……. 27

Fig 4.9– Graph for the mobility in the ZnSnN2 films annealed at different temperatures for 20 min…… 27

Fig 4.10- Graph for the carrier concentration in the ZnSnN2 films annealed at 4500C for different time intervals……. 31

Fig 4.11- Graph for the mobility in the ZnSnN2 films annealed at 4500C for different time intervals……. 31

List of Tables

Table 1 – Lattice parameters calculated from the measured XRD pattern……... 18

Table 2- The values of full width at half maximum and average crystalline sizes of the deposited ZnSnN2 films subjected to RTA at different temperatures……. 21

Table 3- The values of full width half maximum (FWHM) and average crystallite sizes of the as deposited films and films annealed at different conditions……. 22

List of Abbreviations

HRXRD	High Resolution X-Ray Diffraction
RTA	Rapid Thermal Annealing
MBE	Molecular Beam Epitaxy
FESEM	Field Emission Scanning Electron Microscopy

1. Introduction

1.1 Motivation –

Present day energy demands which are of the terawatt scale, drive the search for new visible range, direct bandgap materials that are earth abundant and are lower in cost than the current available options.

The III-nitride group of semiconductor materials GaN, AlN, and InN have been responsible for having a major impact on the industry by enabling technologies like Blu-Ray® DVD technology, ultraviolet lasers, high brightness three color display LED displays, high power electronics and LEDs for replacing incandescent lights[1,2]. There has also been a lot of interest in these materials for solar energy harvesting.

In spite of these advantages, the III-Nitride group of semiconductor materials, especially the $In_{1-x}Ga_xN$ group of alloys have some major drawbacks. One major drawback is that both Gallium and Indium are not earth abundant materials which means that any attempts made to mass produce technologies like photovoltaic modules, LED displays which are made of these materials will be very limited as the costs of these optoelectronic devices will mainly depend on the availability of the raw materials. Another drawback is that Indium is not an environmentally friendly material. It is considered as kind of a heavy metal and is also a potential bio-toxic metal [8].

Thus, in order to find a way to meet the environmental safety needs and also to reduce the production and manufacturing costs, the search is on for the next generation of materials whose optical and electrical properties are similar to their group III-Nitride counterparts.

1.2 Objective

The aim of this thesis is to investigate the suitability of $ZnSnN_2$ compound semiconductor material as an alternative to the III-V group of semiconductor materials. Affordable electronics have always been a significant factor in driving the semiconductor industry, hence the major factors stopping this material from being used as an alternative were discussed in depth. Rapid Thermal Annealing studies were performed to eliminate the high electron concentration of the material. The different properties of the film like surface morphology, electrical properties were also measured. Lastly a relationship between the annealing time, annealing temperature, stability of the films and the electron concentration was established.

2. Background

2.1 Zn-IV-N_2 group materials

The Zn-IV-N_2 group of semiconductor materials are considered widely as potential candidates to replace the group III-Nitrides after a lot of theoretical calculations and experimental results. This new group of Zn-IV-N_2 semiconductors, where IV = Si, Ge or Sn, are made up of only non-toxic, earth abundant and inexpensive elements [9,10]. As reported by the US geological survey, the elements tin and zinc are present in much more abundance than Indium(around 100 times more)[11,12]. This can be seen in the figure shown below –

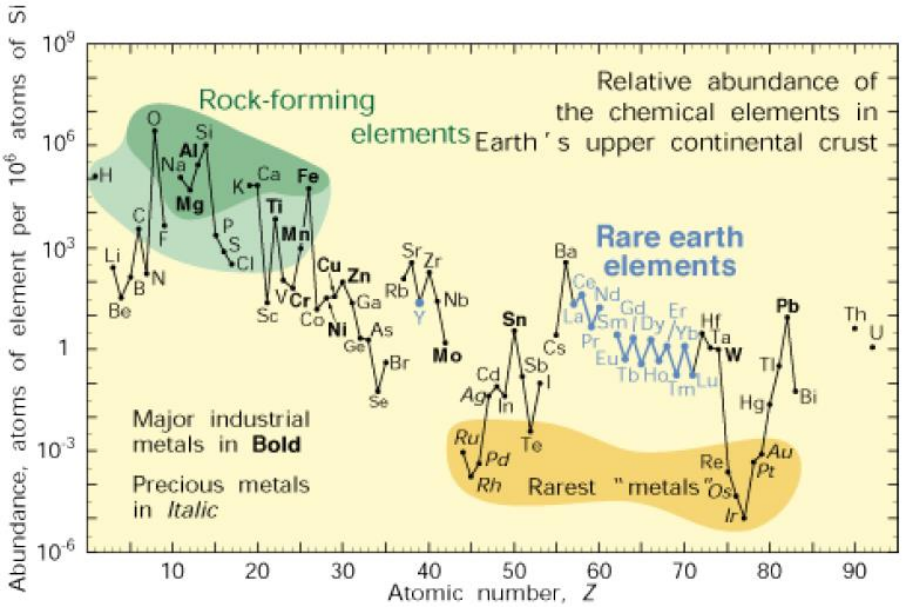

Fig. 2.1- The relative abundance of elements in the Earth's upper continental crust in terms of the US Geology Survey.[22]

The Zn-IV-N_2 group of materials are of great interest due to their relative closeness in electrical and optical properties to the III-N_2 semiconductor materials. The most stable orthorhombic crystal structure for them is conceptually obtained by replacing the group III wurtzite sublattice of the III-

N_2 by an ordered group II and group IV pair of sublattices. Each of the Nitrogen atoms is bound to two group IV atoms and two Zn atoms which helps preserve the nitrogen's octet rule.

The possible space groups for these compounds are $Pbn2_1$, $Pna2_1$ and $Pmc2_1$. Beta-$NaFeO_2$ can be considered as a prototype compound for this new type of materials. The figure below shows the crystal structures of GaN and Zn-IV-N_2 compounds.

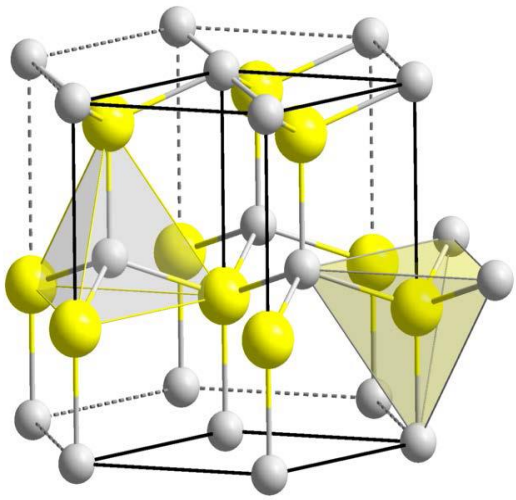

(a)

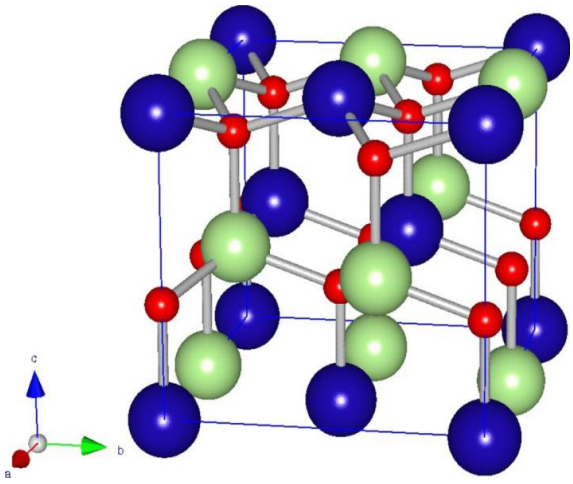

(b)

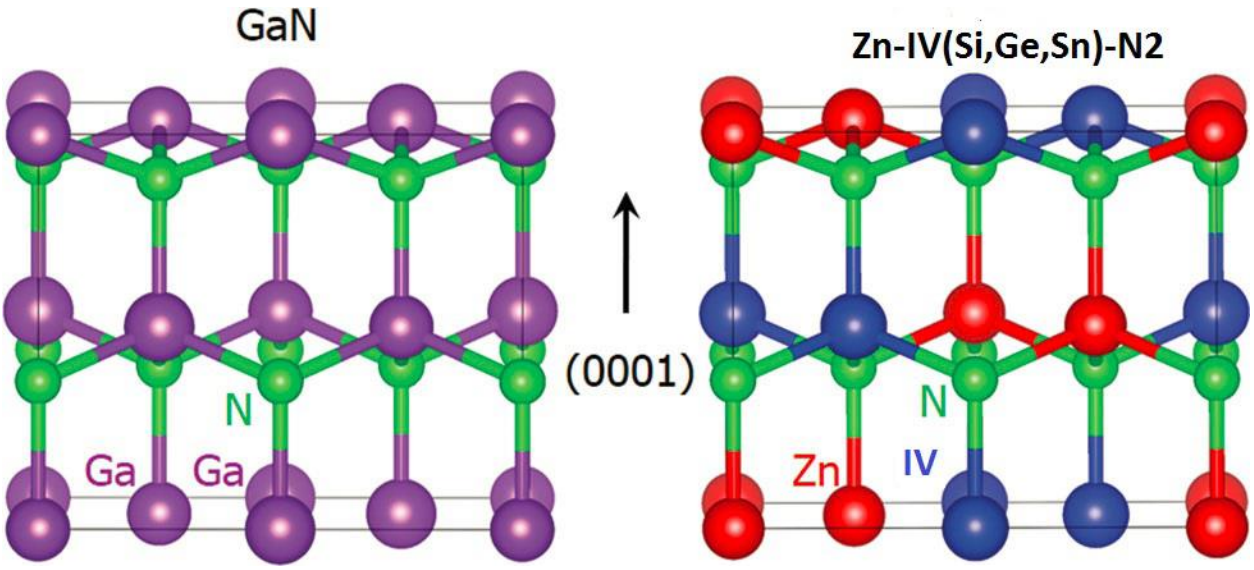

(c)

Fig. 2.2 - Crystal structures of the GaN and Zn-IV-N_2 compounds. (a) A 3-D view of GaN crystal structure: the small light grey spheres are N atoms and the large yellow spheres are Ga atoms [23]. (b) A 3-D view of Zn-IV-N_2 crystal structure: the small red spheres are N atoms, the light green spheres belong to group IV atoms (Si,Sn or Ge) and the dark blue spheres are Zn atoms.[24] (c) The wurtzite GaN and the orthorhombic $ZnSnN_2$ oriented along the (0001) direction.[25]

This new group of Zn-IV-N_2 semiconductor materials are at very early stages of their development as compared to other III-N_2 materials. Their progress is commensurate to the state of III-N_2 group semiconductors around some forty years ago i.e. Zn–IV-nitrides are at an extremely early stage of development, comparable to the state of III-nitrides some four decades ago. There are very few experimental reports available on Zn-IV-N_2 to date [4]. Although the synthesis methods for $ZnGeN_2$ and $ZnSiN_2$ were first reported in 1970, the synthesis of $ZnSnN_2$ was not reported till recently. The Zn(Si,Ge,Sn)N_2 group of semiconductors have the ability to overcome some of the material problems present in the III-Nitride materials. For example, according to recent calculations it has been predicted that the spontaneous polarization of the Zn-IV-Nitride group are much closer to each other than that of the III-Nitrides [5]. Due to this reason there is no need to grow them along nonpolar crystallographic directions, which is difficult and a non-efficient route to avert the spontaneous polarization effect in heterostructures. In addition to this, doping of Zn-IV-N_2 can be achieved in a much easier way compared to III-Nitrides, especially p-type doping, which can be really advantageous for developing shorter wavelength ultra-violet lasers. An example for this is the case of $ZnGeP_2$, which is the Zn-IV-P_2 chalcopyrite analogous to the Zincblende GaP, which was shown to be a p-type material by electron paramagnetic resonance due to presence of Zn-vacancies. This is opposite to GaP which is normally an n-type material when undoped[6]. Additionally, due to the close lattice parameter match with the group III-Nitride materials, it is also possible to synthesize hybrid structures between these two groups of materials. Hence, capitalizing on the unique properties of group Zn-IV-N_2 materials can lead to new applications. An additional point of interest is the fact that the Zn(Sn, Si)N_2 group of alloys cover the ultraviolet

to deep red range of the electromagnetic spectrum completely with non-toxic and earth abundant materials[7].

2.2 Synthesis methods

Understanding how to synthesize these Zn-IV-N_2 compounds of high quality is a very important basis of current research which is focused on realizing the fundamental properties of the material and its device applications.

Five decades ago, Goodman and Pamplin proposed the design and synthesis methods for ternary and quaternary semiconductor materials by the cation mutation in III-V or II-VI binary semiconductor systems[6-8]. One way to achieve this was by replacing two Zn atoms in ZnSe by a single Cu atom and a single In atom. This would mutate ZnSe into a ternary $CuInSe_2$ system, this can be further mutated into a Cu_2ZnSe_4 quaternary system by replacing the two In atoms with Zn and Sn. Both the $CuInSe_2$ and $Cu_2ZnSnSe_2$ systems are highly efficient for light absorption purposes or as semiconductors in thin film solar-cells, which have been of great interest for the last couple of years. In a similar fashion, replacing the two Ga atoms in GaN by Zn and Sn, the GaN compound semiconductor can be mutated into $ZnSnN_2$.

The first time that the preparation of $ZnGeN_2$ was reported was back in 1970. The synthesis method was based on the reaction of Zn_2GeO_4 with NH_3 or by reacting Zn metal with Ge_3N_4[13,14] .

$$8NH_3 + 3Zn_2GeO_4 \rightarrow 3ZnGeN_2 + N_2 + 3Zn + 12H_2O$$

$$Ge_3N_4 + 2Zn \rightarrow 2ZnGeN_2 + Ge$$

Wintenberger et al. were able to study the ordering of cations (Ge and Zn atoms) by using the neutron diffraction method. They reported the structure of $ZnGeN_2$ as orthorhombic with lattice constants: a=6.44A^o, b=5.45A^o and c=5.19A^o[15]. Endo et al demonstrated the first ever growth of single crystal $ZnGeN_2$ in 1992 by using a high pressure synthesis method. But the so obtained $ZnGeN_2$ crystals were opaque and were of fairly low quality with a large amount of impurities present in them[16]. Chemical Vapor Deposition (CVD) or RF Sputtering methods were also used

by some research groups to synthesize $ZnGeN_2$ from 1999 to 2005. Zhu et al. reported to have grown thin films of $ZnGeN_2$ using Metal Oxide Chemical Vapor Deposition (MOCVD). The films were grown on c-plane or r-plane sapphire substrates which were incorporated by a GaN buffer layer in between [17]. Using the experimental results, they were able find out that the so deposited $ZnGeN_2$ thin films featured disorders on the Ge or Zn sublattice. Another group, Misaki et al. used Plasma Enhanced MOCVD in order to obtain $ZnGeN_2$ films on substrates made out of sapphire without the use of a GaN buffer layer [18,19,20]. According to them, the measured bandgap of $ZnGeN_2$ was around 3.3eV. Furthermore, Kikkawa et al. reported the deposition of $ZnGeN_2$ thin films by the RF-Sputter method on silicon and glass substrates. The band gap of the films they obtained was around 3.1eV [21]. A different method for synthesizing ZnGeN2 was proposed by Du et al. in 2008. They used vapor liquid solid (VLS) technique to synthesize polycrystalline $ZnGeN_2$ materials. This method of growth was seen to result in the formation of large needle shaped crystals which were a few microns in diameter and about a few hundred microns in length. The band gap of these materials measured using the photoluminescence technique was found to be around 3.4 eV.

Endo et al used a high pressure method[18] to successfully synthesize $ZnSiN_2$ powder. They used optical absorption analysis to report a measured bandgap of 3.64eV in the synthesized material. A few other groups reported the growth of $ZnSiN_2$ thin films on various substrates.

Cook et al. deposited $ZnSiN_2$ films on a r-plane sapphire substrate using a MOCVD technique. They calculated the refractive indices of these films and determined the band gap to be 4.4 eV[27]. Osinsky et al. deposited $ZnSiN_2$ films on SiC substrates [28] and Mintairov et al. used infrared spectroscopy to repot the IR reflection of ZnSiN2 films deposited on a r-plane sapphire substrate.

The difficulty involved in synthesizing $ZnSnN_2$ groups means there are very few reports related to the preparation of this materials. Recently, Quayle et al. were able to, for the first time, synthesize polycrystalline ZnSnN2 by a plasma-assisted vapor-liquid-solid method (PAVLS)[30]. Using the results from their X-ray diffraction (XRD) measurement, the material is found to be orthorhombic and the obtained lattice parameters were a=6.75 Å, b=5.84 Å and c=5.42 Å. They also used photoluminescence and photoluminescence excitation (PLE) spectroscopy to measure the band gap of this material and found it to be around 1.7eV. Feldberg et al. reported single or textured polycrystalline $ZnSnN_2$ thin films which were grown using the molecular beam epitaxy (MBE) technique. They reported that disorder in the cation sublattice leads to a significant effect on the crystal structure as well as the bandgap. In 2013, Lahourcade et al. synthesized ZnSnN2 thin films on c-plane sapphire/GaN substrates using the RF-sputtering method. The deposited films had an orthorhombic crystal structure with a Pna21 space group. The carrier concentration was measure using Hall measurement and was found to be $10^{21}cm^{-3}$. The optical bandgap based on ellipsometry was found to be around 2eV.

The Figure 2.3 shown below indicates the bandgap as a function of lattice constant "a" for the III-nitride materials and the Zn-IV-N_2 materials. The open symbols in the graph indicate the calculated data and the solid circles represent the experimental results. The experimental values of the bandgaps, lattice constants and bowing parameters of the III-nitrides (AlN, GaN and InN) are from [31] and the experimental parameters for the Zn-IV-N_2 group materials are taken from [25,27,30]

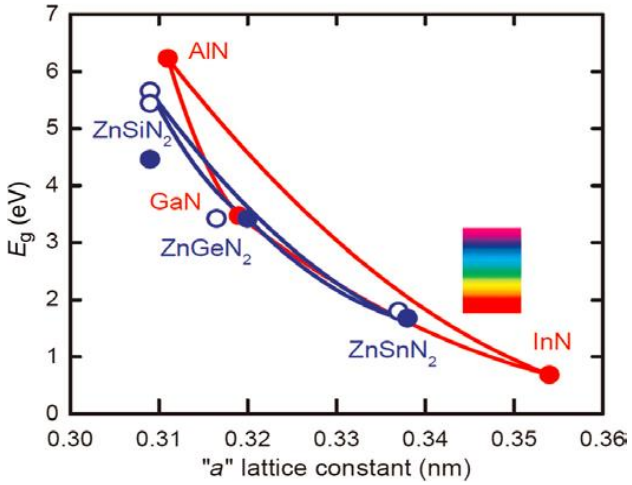

Fig. 2.3 - Band gaps versus lattice constants "a" in III-N and Zn-IV-N_2 nitrides.

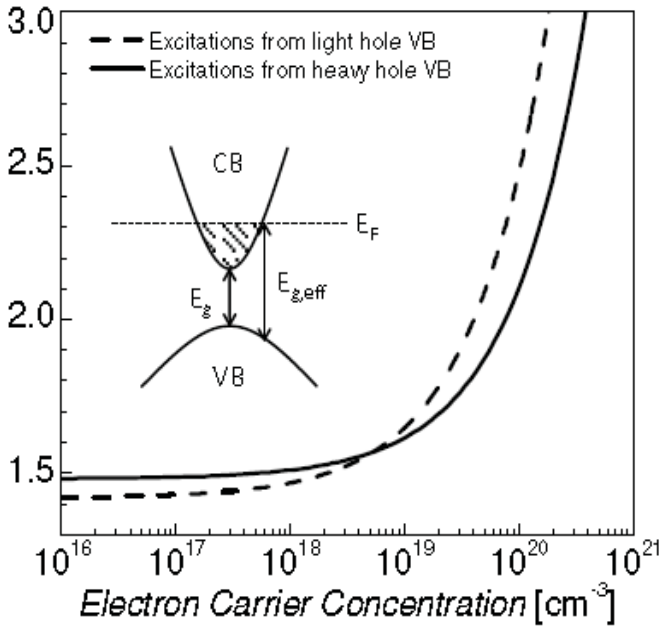

Fig 2.4 - Bandgap variation with carrier concentration in $ZnSnN_2$.

Fig. 2.4 shows the variation of the bandgap with the carrier concentration. As can be seen from the image, the high electron concentration in the material leads to the free electrons filling the bottom of the conduction band which leads to the pinning of the fermi level at energies above the conduction band. The effect leads to an increased value of the measured bandgap value.

3. Preparation and Deposition of $ZnSnN_2$ thin films

3.1 Materials used –

The substrates used in this experiment were (0001) GaN template on c-plane sapphire layers. The GaN layers were grown on the sapphire layers by using MBE at Northrop Grumman Aerospace System (NGAS). The wafers were then diced into smaller samples of 1cm x 1cm dimension each.

3.2 Substrate cleaning –

Standard cleaning procedures were followed for cleaning the samples. The substrates were first cleaned in acetone for 10 minutes by sonication. After this the samples were then cleaned in Isopropanol for 5 minutes by sonication. Lastly all the samples were given a H_2O rinse.

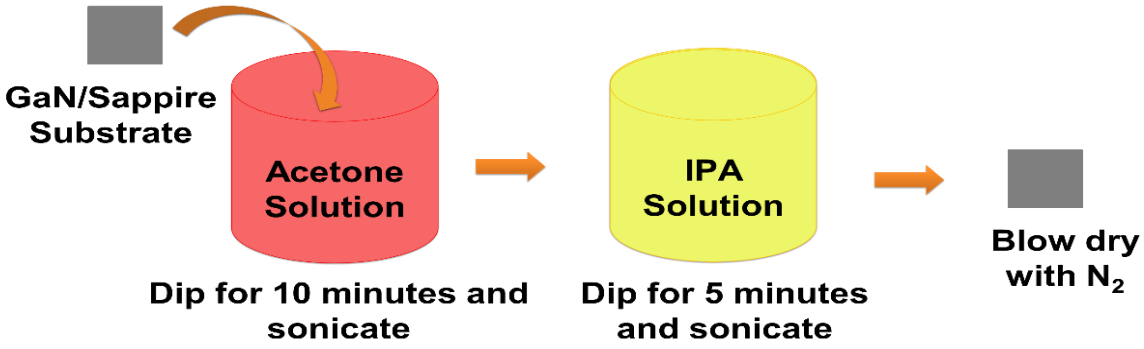

Fig 3.1 – Schematic for the procedure used in Stage 1 of cleaning.

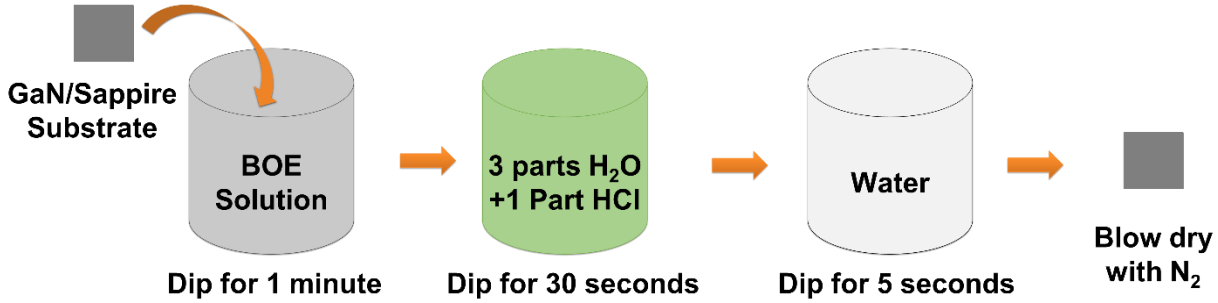

Fig 3.2- Schematic for the procedure used in Stage 2 of cleaning.

The next stage of cleaning involved acid cleaning. The substrates were cleaned in BOE for 1 minute to remove any oxide material that might have formed along with some fraction of the ionic contaminants too. It is important to carry out this step with chemicals of high purity as well as ultra-clean containers as the substrates can be recontaminated really quickly. Next, the substrates were rinsed with H_2O once before being cleaned with a solution containing 3 parts of H_2O + 1 part of HCl (37% by weight) solution for 30 seconds. This ensures the complete removal of any remnant metallic or ionic contaminants from the previous step. Lastly the substrates were all cleaned with H_2O and blow dried by Dry N_2.

3.3 Distinguishing between $ZnSnN_2$ and GaN surfaces

An interesting problem that was faced during the experiments was the inability to determine which surface was which. During the dicing process of the wafers, the cut samples were placed randomly in the substrate holder which made it impossible to distinguish between the Sapphire and GaN layers by visual inspection.

Fig 3.3 – Contact angles of water drops on the GaN and Sapphire sides of the substrate.

A goniometer was used to determine the contact angles of both the surfaces. A water droplet was dropped onto both the surfaces and the contact angle of the water droplet with the surface was measured. The Al_2O_3 side of the substrate had an obtuse angle of contact and the GaN side of the substrate had an acute angle of contact.

After the contact angles were measured the substrates were carefully placed with GaN side up in the substrate holder and cleaned in Isopropanol before depositing $ZnSnN_2$ films onto them.

3.4 Deposition of zinc tin nitride thin films

In this thesis work, polycrystalline $ZnSnN_2$ thin films were deposited by reactive radio frequency (RF) magnetron sputtering system, ULVAC JSP 8000 on c-plane sapphire and (0001) GaN template layer substrates. The sputtering target that was used was a 4 inch diameter alloy of zinc and tin ($Zn_{0.75}Sn_{0.25}$ of 99.995%purity, ACI alloy Inc.) The substrates were held using a rotating metal plate inside the sputtering system at a distance of around 15cm from the target material.

The RF sputtering power used was 300W, and the substrate temperature was set to 400^{o}C to obtain a uniform thin film. The reactive gas inside the sputtering system was a mixture of pure N_2 and Ar with plasma activation. The gas flow rates for each of these gases was 24 sccm and 16 sccm. The base pressure inside the sputtering chamber was around the low range of 10^{-6} Torr (1.0 X10^{-6}Torr to 3.0 x 10^{-6} Torr). A pre-sputtering process was performed prior to the deposition of the films in pure Ar gas atmosphere in order to clean the surface of the target.

After the deposition, the thickness of the deposited film was obtained using a DEKTAK surface profilometer.

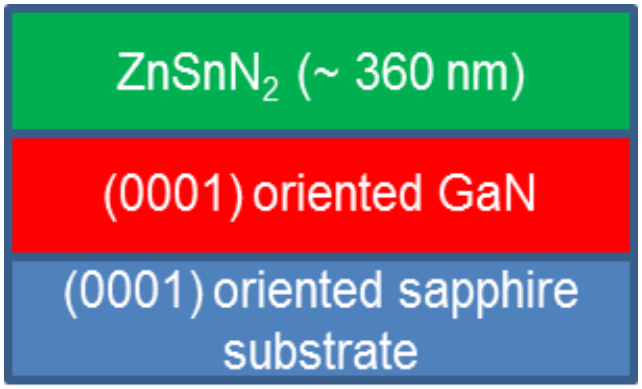

Fig 3.4– Cross-section figure of the deposited $ZnSnN_2$ film and the substrate.

3.5 Rapid Thermal Annealing

Rapid Thermal Annealing is a processing step used widely in the semiconductor industry. The wafers are heated to either activate dopants, facilitate interfacial reaction of the metal contacts, change the states of grown films, drive dopants into different films or to repair damage from ion implantation. The working principle of this technique basically involves heating a wafer rapidly to temperatures as high as 800^{o}C - 900^{o}C, holding it there for a certain amount of time and quenching it as quickly as possible.

The wafer is heated either by using an indirect IR lamp, a hot plate or a hot chuck which is brought near the substrate and the temperature is measured using a thermocouple or a pyrometer. Unlike conventional furnace anneals, the annealing times are really short, with each anneal lasting from a few seconds to a few minutes. The small quench times help to effectively control the diffusion of dopants inside the wafers but can lead to issues like wafer stress and loss of process uniformity.

The $ZnSnN_2$ films in this work were first deposited at 400^{o}C and were subjected to Rapid Thermal Annealing treatment for 20 minutes at different temperatures from 350^{o}C to 550^{o}C with 50^{o}C intervals. The films were also subjected to RTA treatment at 450^{o}C for different time intervals from 20, 40, 60 to 90 minutes and their properties were studied.

4. Characterization of the $ZnSnN_2$ thin films

4.1 High resolution X-Ray Diffraction –

X-ray diffraction is a method used to characterize epitaxial layers in semiconductor materials which are used in electronic or optical devices. X-rays are produced by suddenly decelerating electrons moving at high velocities by using a target. These decelerated electrons at the target produce a continuous spectrum of radiation along with sharp intensity peaks. These sharp peaks are due to the k-shell electrons being knocked out of their shells which leads to a plethora of other electrons filling the empty shells and releasing energy. This phenomena leads to something known as characteristic wavelength of the radiation K α to have a higher intensity than normal.

Usually during the coupled scan or 2theta-omega (2θ-ω) scan, the source is fixed and the detector and samples are rotated. This type of a scan is generally used to study parameters like lattice mismatch, relaxation and composition which effect the position of the Bragg peak. Whereas rocking curves or omega (ω) scans have the samples tilted while the detector is set at an angle during which the omega changes. The rocking curve is primarily used to study the dislocation and defects which are primarily linked to the full width at half maximum (FEHM).

The $ZnSnN_2$ thin films' X-Ray Diffraction (XRD) measurements were performed using a PANalytical X'Pert Pro x-ray powder diffractometer. A Cu Kα radiation source was used with a sealed proportional detector which was equipped with an X'Pert highscore software.

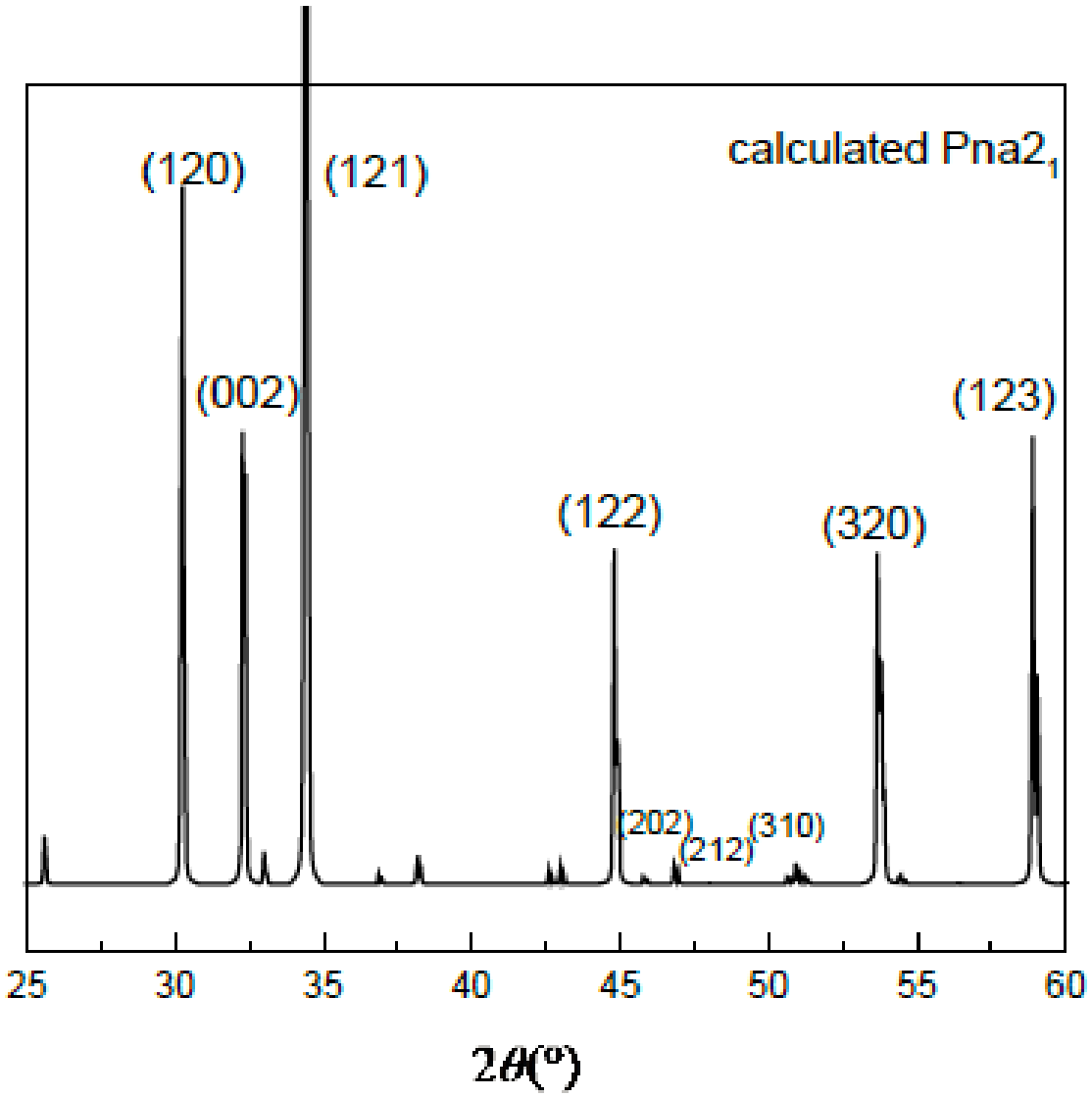

Fig 4.1 – Calculated XRD pattern for the deposited $ZnSnN_2$ films.

In the figure 4.1 shown above we can see the calculated powder diffraction spectra for the $ZnSnN_2$ which is based on the orthorhombic crystal structure in the Pna21 space group. The growth conditions for the films are as follows- The substrate temperature was set to around 400°C and the ratio of $N_2/(N_2+Ar)$ ratio of 50%. It can be seen that the dominant characteristic peaks from the experimental data match with peaks in the calculated pattern, from which we can confirm that the structure of the deposited $ZnSnN_2$ films is orthorhombic. The lattice parameters for the material are listed in the table below and can be calculated as follows[32] -

Bragg's equation: $\lambda = 2d \sin \theta$

Where λ is the X-ray wavelength (here, the Cu Kα1 characteristic line is 1.54Å); d is the lattice spacing distance; and finally θ is the diffraction angle.

Peak Positions	Milled Index	Lattice spacing	Lattice parameters		
2θ (°)	h k l	d (A°)	a (A°)	b (A°)	c (A°)
30.4536	1 2 0	2.9328			
32.4756	0 0 2	2.7547			
34.5657	1 2 1	2.5926	5.855 ± 0.0112	6.749 ± 0.0238	5.527 ± 0.0143
54.1137	3 2 0	1.6934			
59.3385	1 2 3	1.5561			

Table 1 – Lattice parameters calculated from the measured XRD pattern.

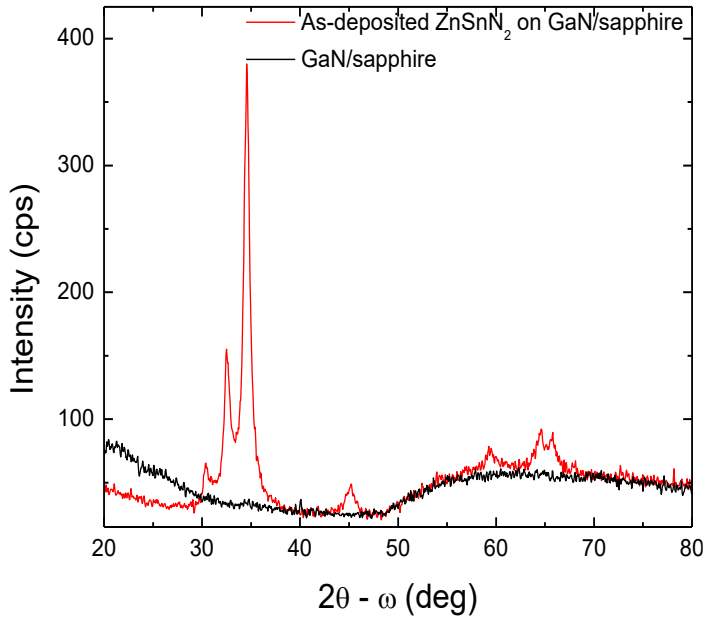
As-deposited ZnSnN2 on GaN/sapphire
GaN/sapphire
Intensity (cps)
2θ - ω (deg)

(a)

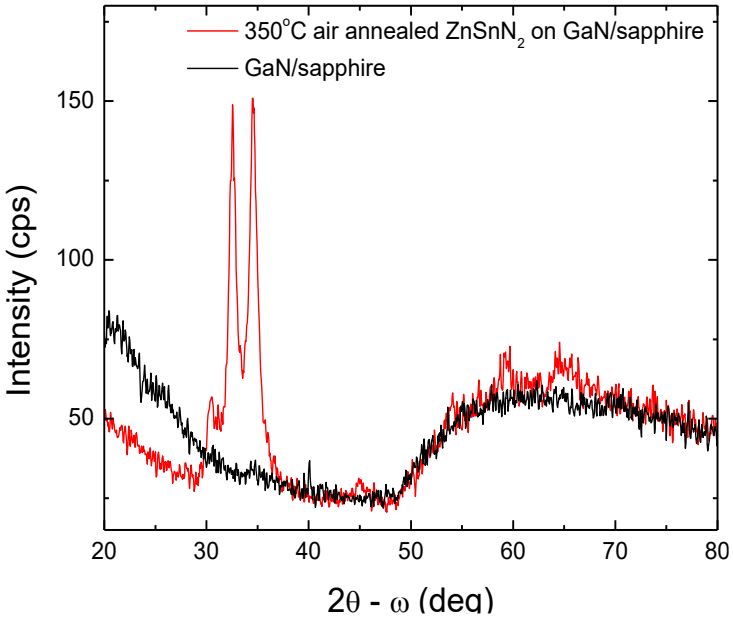
350°C air annealed ZnSnN2 on GaN/sapphire
GaN/sapphire
Intensity (cps)
2θ - ω (deg)

(b)

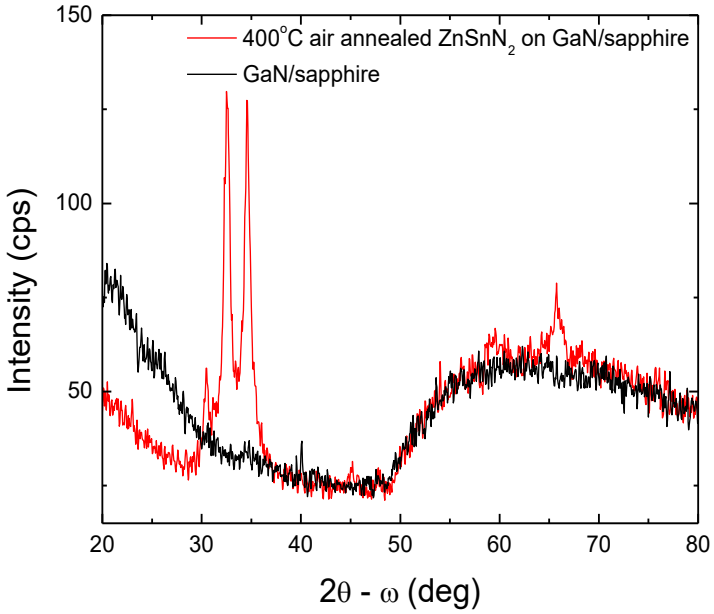
400°C air annealed ZnSnN2 on GaN/sapphire
GaN/sapphire
Intensity (cps)
2θ - ω (deg)

(c)

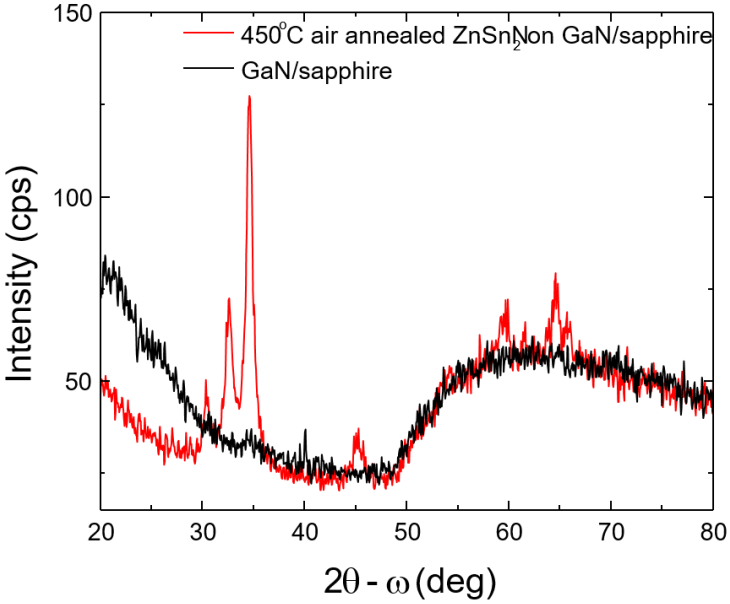
450°C air annealed ZnSnN2 on GaN/sapphire
GaN/sapphire
Intensity (cps)
2θ - ω (deg)

(d)

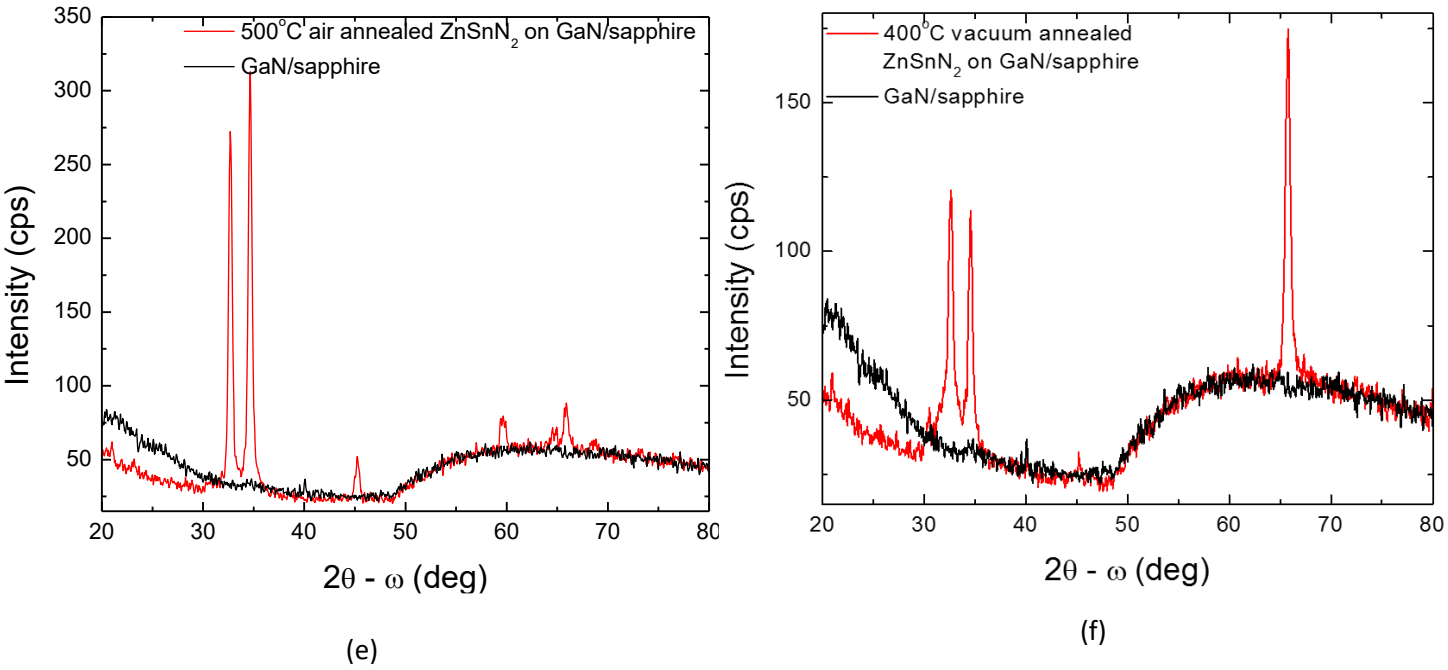

Fig 4.2– Measured XRD patterns for a) Sample wit as deposited $ZnSnN_2$ film b) Samples subjected to RTA at 350°C. c) Samples subjected to RTA at 400°C d) Samples subjected to RTA at 450°C e) Samples subjected to RTA at 500°C f) samples subjected to vacuum anneal at 400°C.

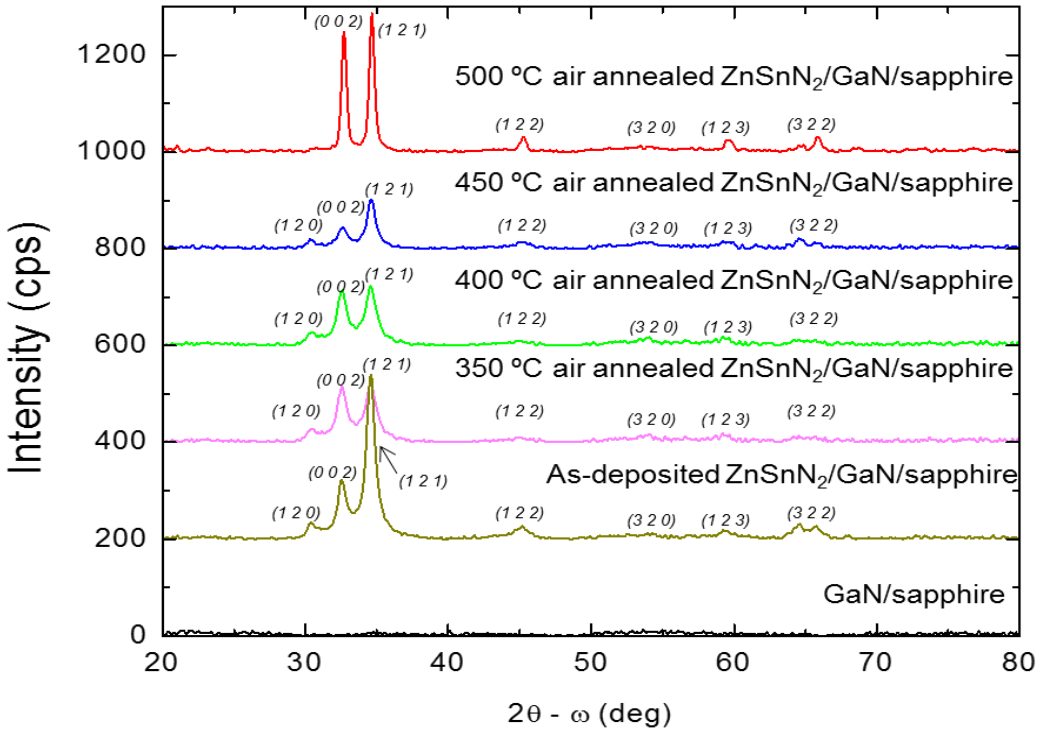

Fig 4.3– Background stripped XRD patterns of the samples subjected to RTA at various temperatures.

	(0 0 2)		(1 2 0)		(1 2 2)		Averaged grain size (nm)
	FWHM (deg)	Grian size (nm)	FWHM (deg)	Grian size (nm)	FWHM (deg)	Grian size (nm)	
As-deposited	0.886	9	0.783	11	1.127	8	9
350 ºC air annealed	0.876	9	0.958	9	1.444	6	8
400 ºC air annealed	0.888	9	0.964	9	1.441	6	8
450 ºC air annealed	0.927	9	0.702	12	1.676	5	9
500 ºC air annealed	0.427	19	0.429	19	0.538	16	18

Table 2- The values of full width at half maximum and average crystalline sizes of the deposited $ZnSnN_2$ films subjected to RTA at different temperatures.

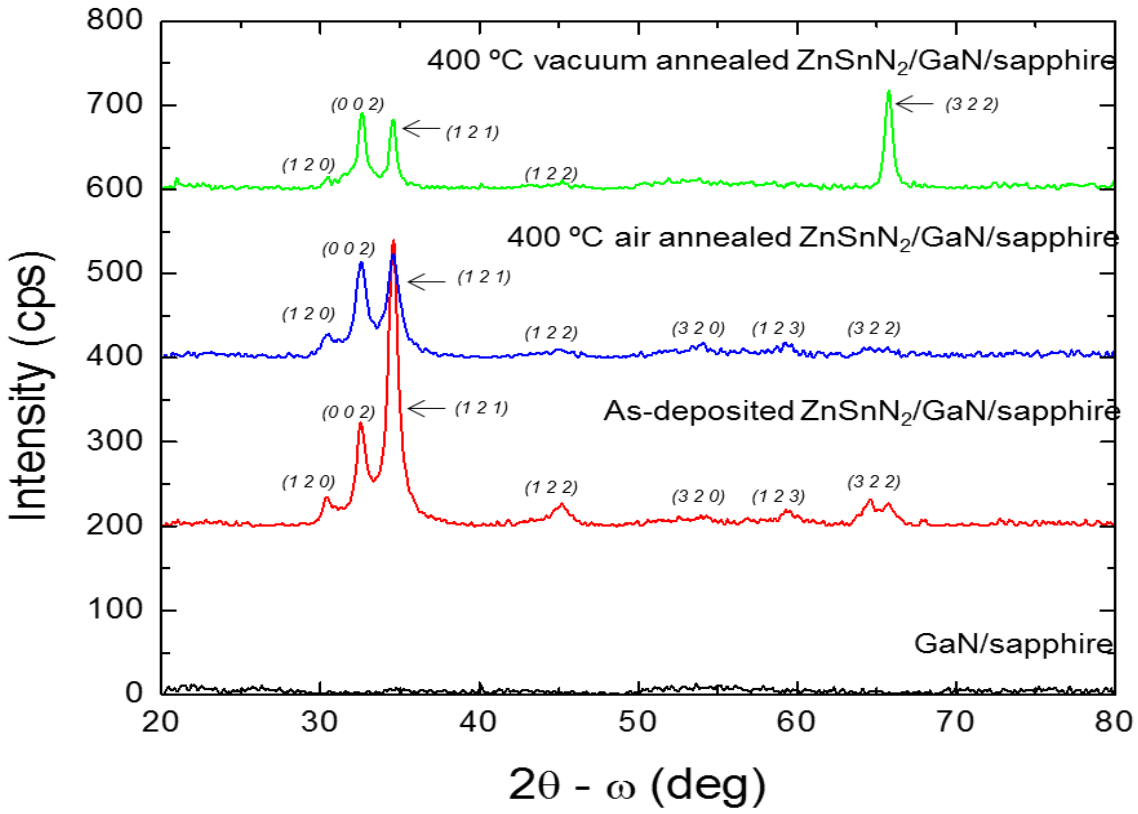

Fig 4.4 - 2θ – ω vs Intensity for $ZnSnN_2$ samples annealed a different conditions.

	(0 0 2)		(1 2 0)		(1 2 2)		Averaged grain size (nm)
	FWHM (deg)	Grian size (nm)	FWHM (deg)	Grian size (nm)	FWHM (deg)	Grian size (nm)	
As-deposited	0.886	9	0.783	11	1.127	8	9
400 ºC air annealed	0.888	9	0.964	9	1.441	6	8
400 ºC vacuum annealed	0.572	14	0.513	16	0.823	10	13

Table 3- The values of full width half maximum (FWHM) and average crystallite sizes of the as deposited films and films annealed at different conditions.

4.2 Surface Morphology –

Scanning electron microscopy (SEM) was used to investigate the surface characteristics of the deposited $ZnSnN_2$ films. The scanning electron microscope images were obtained on a FEI Nova NanoSEM230 field emission scanning electron microscope.

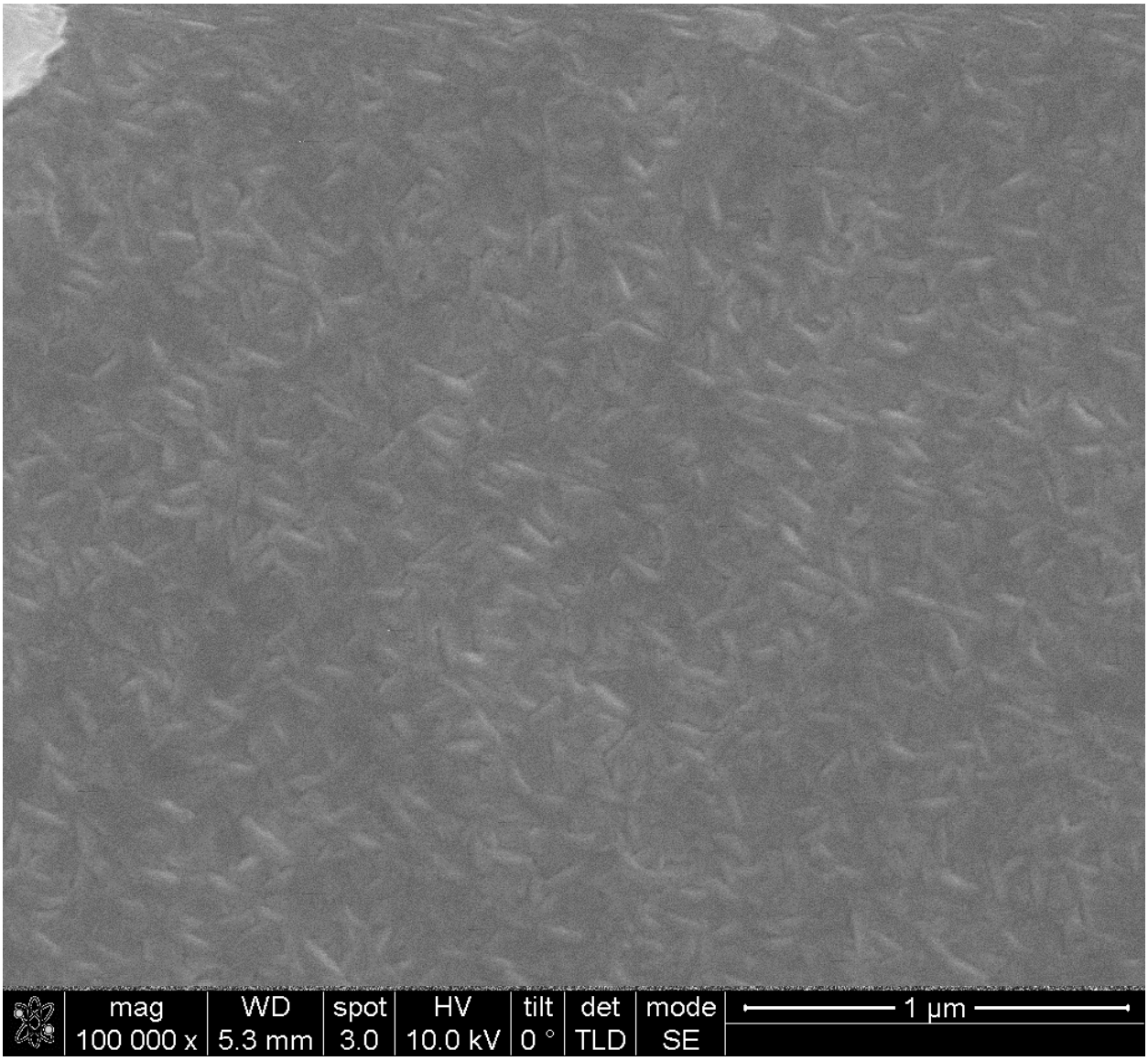

Fig 4.5- SEM image of ZnSnN2 thin films deposited at the substrate temperature of 400 ˚C and vacuum annealed for 4 hours with N2/(N2+Ar) ratio of 50%. (SEM conditions are HV=10kV, WD=5.3 mm, spot size=3.0, and scale bar=1um).

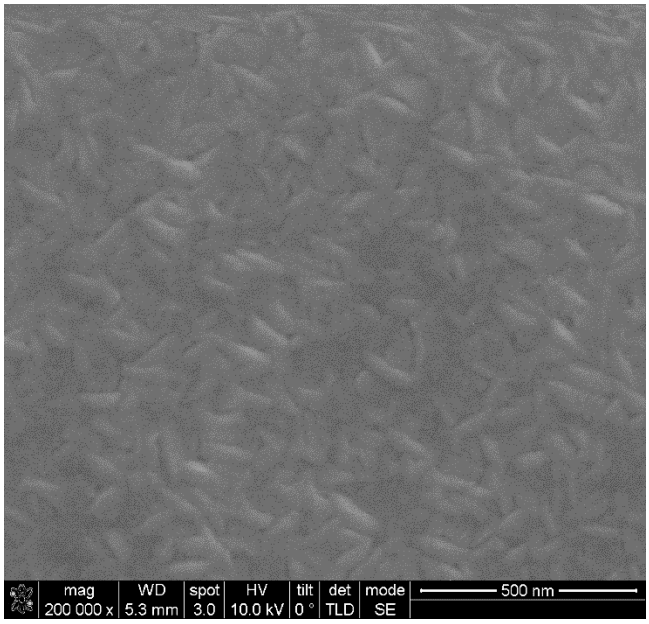

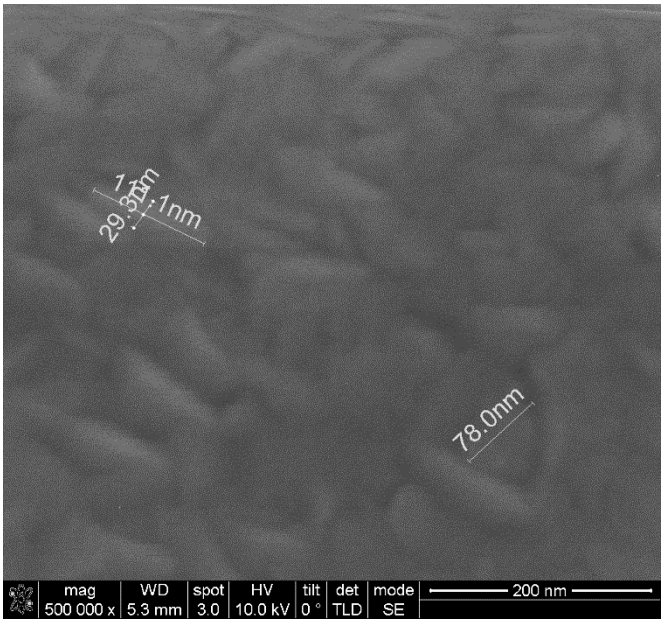

Fig 4.6- SEM image of ZnSnN2 thin films deposited at the substrate temperature of 400 ˚C and vacuum annealed for 4 hours with N2/(N2+Ar) ratio of 50%. (SEM conditions are HV=10kV, WD=5.3 mm, spot size=3.0, and scale bar=500nm and 200nm).

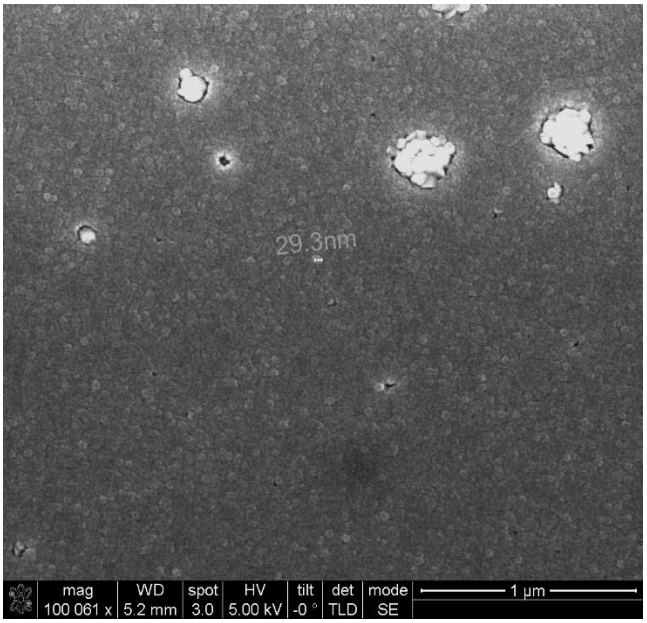

Fig 4.7 - SEM image of ZnSnN2 thin films deposited at the substrate temperature of 400 ˚C and rapid thermal annealed at 450^{o}C for 20 minutes with N2/(N2+Ar) ratio of 50%. (SEM conditions are HV=10kV and 5kV, WD=5.3 mm, spot size=2.0 and 3.0, and scale bar=1um).

The SEM images show that the average grain size after deposition is really small and the grain orientation is very random. This is expected given the deposition was done by sputtering. RF Sputtering is a deposition process which occurs in a plasma and is a non-equilibrium process. Due to the low ion energies from frequesnt collisions with other atoms and high pressure inside the chamber, the mobility of the surface atoms is very limited. Due to the low mobility of the adatoms, the coalescence process is limited kinetically which reulsts in smaller grain sizes distributed in many different orientaitons.

4.3 Electrical properties

Hall Effect measurements are used to characterize semiconductors and provides information on the majority type concentration, mobility, and resistivity. These measurements are commonly used to measure the channel conductivity in most semiconductor devices.

The Hall Effect measurements are based on the measurements of induced voltage of a samples in magnetic field oriented perpendicular to samples surface. The electrons moving in the magnetic field are influenced by the Lorentz Force[37]:

$$F = q \cdot (v_d \times B)$$

Where q is elementary charge (1.602×10^{-19} C), v_d is drift velocity, and B is the inductance of the magnetic field. Using the relationship between current density $J = env_d$ for electrons and electric field (E):

$$\frac{J}{en} B_z = -E_y$$

And the Hall factor (RH):

$$R_H = \frac{1}{en}$$

Conductivity (σ_n) is measured and the Hall mobility (μ_n) for electrons can be determined: [6]

$$\mu_n = \frac{\sigma_n}{en}$$

In our experiments, Hall Effect measurement was performed to measure the electrical properties of the deposited $ZnSnN_2$ film like its carrier concentration and mobility. The room temperature Hall Effect measurements were performed in a DHE-21 Hall system from SES Instruments Pvt. Ltd, using a standard four point Vand der Pauw contact layout[33]. For good electrical measurements we generally need good ohmic contacts so a small layer of InP was used on the $ZnSnN_2$ films in the Van der Pauw pattern before the electrical measurements were carried out. The magnitude of the magnetic field was set to around 2800G in the Hall system. A magnetometer was used to measure the magnetic fields. The samples that were investigated were grown on c plane sapphire substrates with a (0001) GaN template. The obtained films were then subjected to rapid thermal annealing at different temperatures varying from 350 to 550^{o}C at which point the films were observed to degrade.

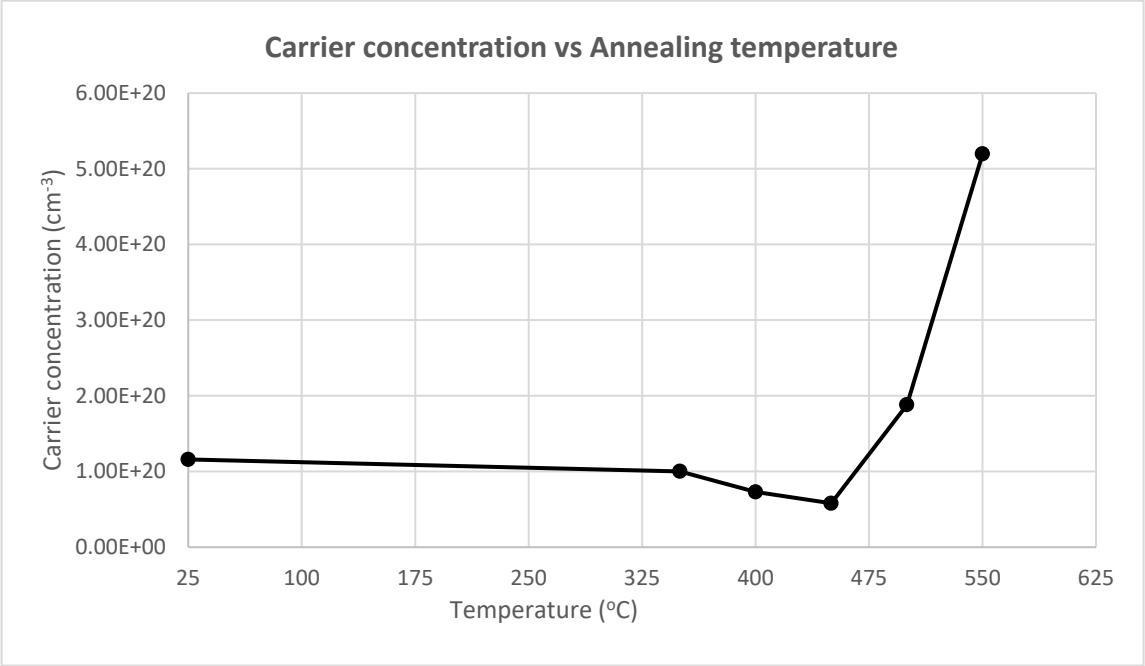

Fig 4.8 – Graph for the carrier concentration in the $ZnSnN_2$ films annealed at different temperatures for 20 min.

The hall measurements showed that all the samples demonstrated n-type semiconductor characteristics. For most samples, the carrier concentration was found to be in the range of 10^{20} -10^{21} cm-3 and the resistivity was found to be between 10^{-2} Ω-cm and 10^{-3} Ω-cm calculate these values, and the values of mobility are in the range of 4.6 to 15.3 $cm^2V^{-1}s^{-1}$. These results are consistent with the data reported in previous works[30,31].

Figure 4.9 reflects the relationship between the mobility values of $ZnSnN_2$ at different annealing temperatures. The carrier concentration was observed to have no significant change till 325°C, but decreased thereafter as the annealing temperature was increased till 450°C. This can be attributed to a reduction in the concentration of Zn-Sn anti-sites which are a major reason for the high carrier concentration in this material. At this point the films started to show degradation and annealing at higher temperatures caused a sharp increase in the carrier concentration.

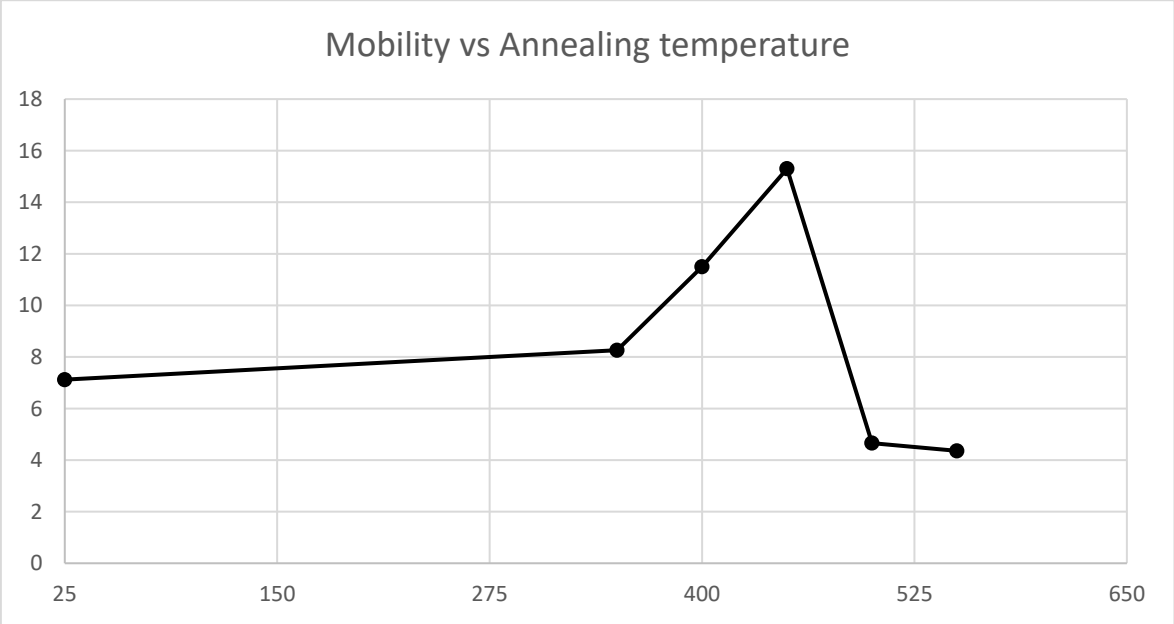

Fig 4.9– Graph for the mobility in the $ZnSnN_2$ films annealed at different temperatures for 20 min.

The measured value of Hall mobility was observed to increase initially with increase in the annealing temperature and reach a maximum value of 15.3 $cm^2V^{-1}S^{-1}$ at 450^{o}C and later on decreased to around 4.36 $cm^2V^{-1}S^{-1}$ at 550^{o}C. The Hall mobility first increased then decreased with increasing temperatures from 275 ˚C to 400 ˚C. To understand this behavior, we have to take a look at the carrier transport phenomenon in $ZnSnN_2$ films.

The relationship between Hall mobility, carrier concentration and resistivity is illustrated using the following equation:

$$\mu = \frac{1}{\rho n e}$$

Here μ is the hall mobility, ρ is the resistivity, n is the carrier concentration and e is the free electron charge (1.609×10^{-19}C). It is a well-known fact that polycrystalline semiconductor materials have mobility values which are dependent on the ionized impurity scattering and grain boundary scattering[33,34]. In our case, as the annealing temperature increases from 350°C to 450°C, the thin films' crystallinity increases. The increase in the average grain size in the deposited film can also be verified from the XRD observations where the grain size increased from 8nm at 350°C to around 11nm at 450°C. So the mobility increases in this temperature range along with the carrier concentration which may suggest that the mobility is affected more by grain boundary scattering. The mobility was observed to decrease thereafter till 550°C. Although this might seem counter-intuitive from a materials standpoint, it can be explained by the following mechanism - In the temperature range of 500°C – 550°C, the ionized impurity scattering becomes the dominant factor in determining hall mobility. As we go to higher and higher temperatures, more and more defects are activated, but due to the rapid cooling process in our experiment, the defects cannot be eliminated and this leads to a reduction in the mobility of the film.

Another explanation for this decrease in mobility at high temperatures can be found in a recently published computational work on the compositional inhomogeneity present in multinary and tetrahedrally bonded semiconductor materials[36]. Drawing from that work, the compositional inhomogeneity described there essentially refers to an entropy driven tendency for all non-octet rule preserving tetrahedra to cluster together when subjected to heat treatment or even during high

temperature growth. This kind of clustering was shown to have resulted in charge localization which in turn leads to an increase in concentration of charge scattering centers and subsequently leading to a decrease in the mobility of the material. The $ZnSnN_2$ films which were deposited by RF sputtering undoubtedly contain a large degree of cation disordering from the beginning. When these films were subjected to annealing treatment at high temperatures, it may have motivated the formation of motifs which lower the mobility. One potential way to avoid this clustering of motifs while still being able to subject the grown films to annealing treatments would be to grow the initial film in such a way that the growth process will encourage order like for example growing them on lattice matched substrates.

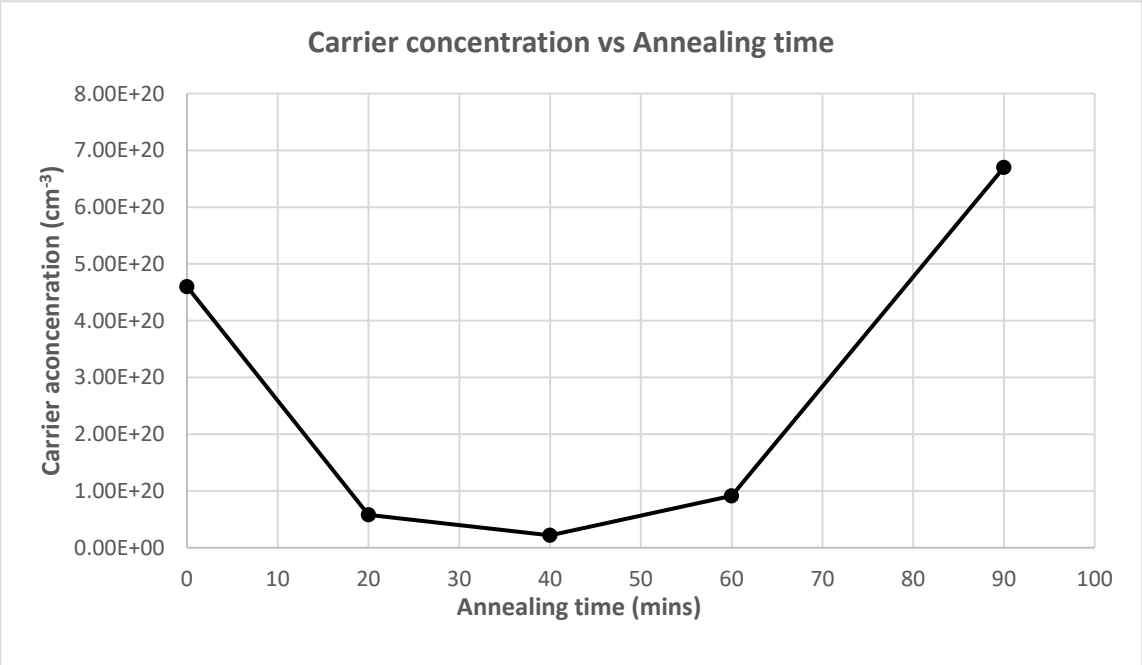

Fig 4.10- Graph for the carrier concentration in the $ZnSnN_2$ films annealed at 450^0C for different time intervals.

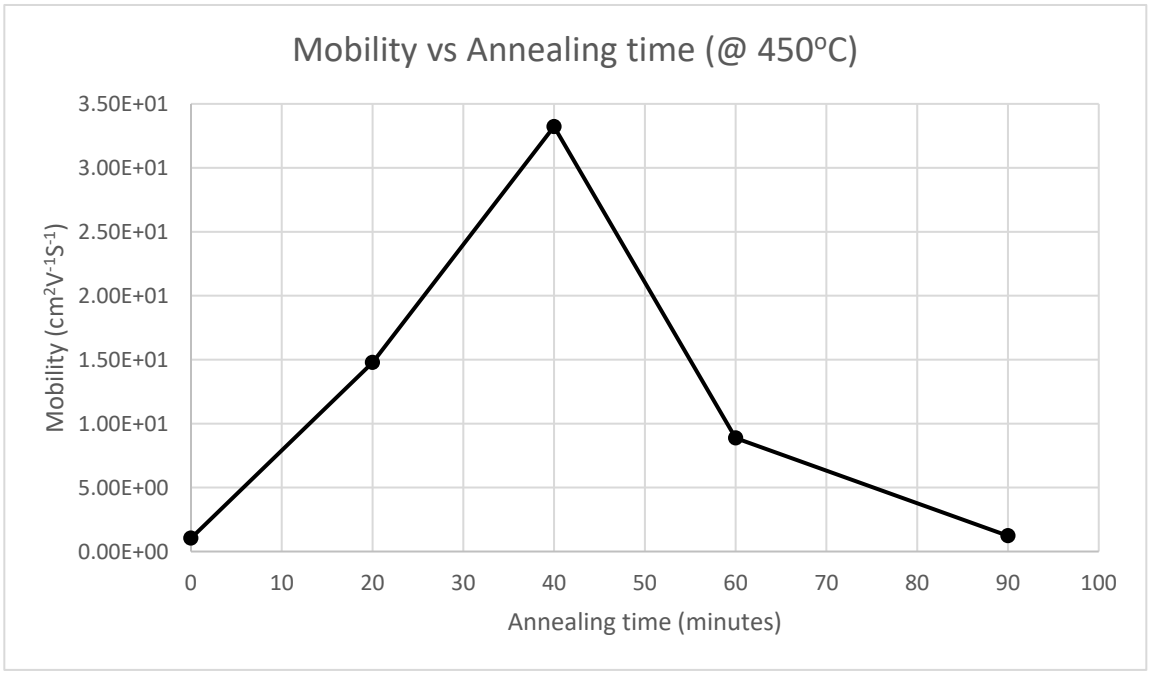

Fig 4.11- Graph for the mobility in the $ZnSnN_2$ films annealed at 450^0C for different time intervals.

The effect of different annealing times on the carrier concentration and mobility was also studied as shown in the figures above. A downward trend in the carrier concentration was observed with increasing annealing time and after around 40 minutes of annealing, the carrier concentration started to increase. The hall mobility first increased with increasing annealing time and then decreased.

The aim of this dissertation was to determine the suitability of $ZnSnN_2$ as an absorber layer for next generation solar cells. As stated earlier, one of primary obstacles for this has been the presence of a high electron concentration in this material. In a recent study by Atwater et al.[43] they reported that one of the primary reasons for the high electron concentration of the material is due to the presence of defects in the films. The donor defects like Sn_{Zn} antisite defects (Sn which has 2 more valence electrons than Zn, substituting Zn atoms), Zn_i (Zn on the interstitial site which is surrounded by four N atoms) and V_N (Nitrogen vacancy) have much lower formation energies than acceptor defects like Zn_{Sn} (Zn substituting Sn atoms), V_{Zn} and N_i. This leads to a predominantly intrinsic n-type doping in this material. The purpose of annealing in this study was to try to eliminate these defects in the films deposited using sputtering and thereby decreasing the disorder in the lattice structure.

Hall Effect measurement was used in order to measure the change in the free electron concentration after the annealing process. However the results above indicate that the lowest achieved value of carrier concentration in this work are higher than the values that were expected at the beginning. This can be explained using the fact that the presence of point defects is only one of the factors contributing to the n-type doping of the material.

In the same study, Atwater et al.[43] reported that another likely factor influencing the properties of $ZnSnN_2$ is the coexistence of secondary phases in the grown films. Due to its low heat of formation, the $ZnSnN_2$ films synthesized are quite unstable and there is a high chance of secondary phases like Zn and Sn metals and Zn_3N_2 to be present in the grown films. The coexisting Zn and Sn metal phases may also be a reason for the high electron concentration. So methods to avoid the formation of these secondary phases are critical for the future developments and applications of the $ZnSnN_2$ semiconductor material.

5. Conclusion

The work done in this thesis was mainly centered on the properties of $ZnSnN_2$ films. Different properties like crystal structure, lattice parameters and the carrier concentration were investigated. Post growth rapid annealing studies were performed to determine the suitability of this material as a viable option to replace some of the III-V materials. The main achievements in this work are listed as follows:

(1) $ZnSnN_2$ films were successfully deposited on c-plane sapphire and (0001) GaN substrates using the reactive RF-sputtering method. The growth conditions were optimized to get smooth and uniform $ZnSnN_2$. Smooth films are usually preferred as the absorber layers in solar cells so as to maximize the ratio of the illuminated area to the area of the interface.

(2) The obtained $ZnSnN_2$ films were then subjected to Rapid Thermal Annealing and the annealed films were characterized using X-ray diffraction, Hall measurement and SEM.

(3) A relationship between the annealing parameters and electrical properties of this material like mobility, carrier concentration and resistivity was established for the first time.

(4) It was shown that the combination of RF Sputtering plus Rapid Thermal Annealing is a way of improving the properties of the material in terms of the carrier concentration, and is a step in the right direction.

Quite non-intuitively, it has been shown that the mobility of this material initially increased as a function of temperature but started to decrease at higher annealing temperatures. This was attributed to the fact that at lower temperatures the more dominant phenomenon affecting mobility values was grain boundary scattering and at high temperatures, ionized impurity scattering was the

more dominant mechanism. The increase in mobility at high temperatures was also a likely indicator of non-octet rule preserving motif clustering in this material. This highlights the need to deposit high quality $ZnSnN_2$ films which have a minimal initial disorder before going for post growth annealing treatment.

The free electron concentration in this material was found to initially decrease with annealing temperature reinforcing the fact that the anti-site defects stated as a possible reason for the high electron concentration were indeed a major factor affecting the carrier concentration in this material. Although the carrier concentration increased at high annealing temperatures, it is likely from the degradation of the film.

In conclusion the work done here suggests that $ZnSnN_2$ has a tremendous potential as an earth abundant semiconductor material to be used as an absorber layer in solar cells and other optoelectronic applications. Further work to develop controlled n and p-type doping in this material is required to truly realize the potential of this material.

References

[1] M.A. Khan: AlGaN multiple quantum well based deep UV LEDs and their applications. Phys. Status Solidi A 203, 1764 (2006).

[2] M.M. Mills: The LED illumination revolution. Forbes, 02/27/2008.

[3] J. Wu, W. Walukiewicz, K.M. Yu, W. Shan, J.W. Ager, III, E.E. Haller, H. Lu, W.J. Schaff, W.K. Metzger, and S. Kurtz: Superior radiation resistance of In1−xGaxN alloys: Full-solar-spectrum photovoltaic material system. J. Appl. Phys. 94, 6477 (2003).

[4] A. Punya, W.R.L. Lambrecht, and M. van Schilfgaarde: Quasiparticle band structure of Zn-IV-N2 compounds. Phys. Rev. B 84, 165204 (2011).

[5] L. Lahourcade, N.C. Coronel, K.T. Delaney, S.K. Shukla, N.A. Spaldin, and H.A. Atwater: Structural and optoelectronic characterization of RF sputtered ZnSnN2. Adv. Mater. 25, 2562 (2013).

[6] L.E. Halliburton, G.J. Edwards, M.P. Scripsic, M.H. Rakowsky, P.G. Schunemann, and T.M. Pollak: Electron-nuclear double resonance of the zinc vacancy in ZnGeP2. Appl. Phys. Lett. 66, 2670 (1995).

[7] L.E. Halliburton, G.J. Edwards, M.P. Scripsic, M.H. Rakowsky, P.G. Schunemann, and T.M. Pollak: Electron-nuclear double resonance of the zinc vacancy in ZnGeP2. Appl. Phys. Lett. 66, 2670 (1995).

[8] Gwinn, W. M. Qu, W. Bousquet, R. W. Price, H. Shines, C. J. Taylor, G. J. Waalkes, M. P. Morgan, D. L. (2014). “Macrophage Solubilization and Cytotoxicity of Indium-Containing

Particles as in vitro Correlates to Pulmonary Toxicity in vivo", Toxicological Sciences. doi:10.1093/toxsci/kfu273

[9] T. R. Paudel and W. R. L. Lambrecht, "First-principles calculations of elasticity, polarization-related properties, and nonlinear optical coefficients in Zn-IV-N2 compounds", Phys. Rev. B., 79(24) , 245205, 2009

[10] A. Punya, W. R. L. Lambrecht , and M. van Schilfgaarde, "Quasiparticle band structure of Zn-IV-N2 compounds", Phys. Rev. B., 84, 165204, 2011.

[11] "Rare Earth Elements—Critical Resources for High Technology, 087-02, U.S. Geological Survey Fact Sheet", [Online]. Available: http://pubs.usgs.gov/fs/2002/fs087-02/.

[12] W.C.Hsu, "Processing-Dependent Growth Mechanisms and Performance Improvement of Kesterite Solar Cells", PhD thesis, University of California at Los Angeles, 2014

[13] B.Gil, "III-Nitride Semiconductors and their modern devices", Oxford university press, UK, 2013, pp 519-585.

[14] M.Maunaye and J.Lang, "Preparation et Proprietes de ZnGeN2", Mater. Res. Bull, 5:793, 1970

[15] M.Wintenberger, M.Maunaye, and Y. Laurent, "Groupe spatial et ordre des atoms de zinc et de germanium dans ZnGeN2", Mat. Res. Bull., 1:1049, 1973.

[16] T. Endo, Y. Sato, H. Takizawa , M. Shimada, "High pressure synthesis of new compounds, ZnSiN2 and ZnGeN2 with distorted wurtzite structure", J. Mater. Sci. Lett.,11 , 424 , 1992.

[17] L.D.Zhu, P.H.Maruska, P.E.Norris, P.W.Yip and L.O.Bouthillette, “Epitaxial growth and structural characterization of single crystalline ZnGeN2”, MRS Internet J.Nitride Semicond. Res., 4S1:G3.8, 1999.

[18] T.Misaki, K. Tsuchiya, D. Sakai, A.Wakahara, H. Okada, and A. Yoshida, “Growth and characterization of ZnGeN2 by using remote-plasma enhanced metalorganic vapor phase epitaxy”, Phys. Stat. Solidi., 0:188-191, 2000

[19] T. Misaki, A. Wakahara, H. Okada and A. Yoshia, “Optical properties of ZnGeN2 epitaxial layer”, Phys. Stat. Solidi (c), 0:2890-2893, 2003

[20] T. Misaki, A. Wakahara, H. Okada, and A. Yoshida, “Epitaxial growth and characterization of ZnGeN2 by metalorganic vapor phase epitaxy”, J.Cryst. Growth, 260:1049, 2004.

[21] S. Kikkawa and H. Morisaka, “RF-sputter deposition of Zn-Ge nitride thin films”, Solid State Commun., 112:513-515, 1999.

[22] “Rare Earth Elements—Critical Resources for High Technology, 087-02, U.S. Geological Survey Fact Sheet”, [Online]. Available: http://pubs.usgs.gov/fs/2002/fs087-02/.

[23] http://en.wikipedia.org/wiki/Gallium_nitride

[24] A.Boochun, W.R.Lambrecht, “First-principles study of the elasticity, piezoelectricity, and vibrational modes in LiGaO2 compared with ZnO and GaN”, Phys.Rev.B., 81, 235214, 2010

[25] S.Y.Chen, P.Narang, H.A.Atwater, L.W.Wang, “Phase Stability and Defect Physics of a Ternary ZnSnN2 Semiconductor: First Principles Insights”, Adv. Mater., 26, 311-315, 2014.

[26] B. P. Cook, H. O. Everitt, I. Avrutsky, A. Osinsky, A. Cai, and J. F. Muth, “Refractive indices of ZnSiN2 on r-plane sapphire”, Appl.Phys.Lett., 86(121906), 2005

[27] A. Osinsky, V. Fuflyigin, L. D. Zhu, L.D. Goulakov, J. W. Graff, and E. F. Schubert, “ New concepts and preliminary results for SiC bipolar transistors: ZnSiN2 and ZnGeN2 heterojunction emitters”, In 2000 IEEE/Cornell Conference on High Performance devices, page 168-172. IEEE, 2000

[28] A. Mintairov, J. Merz, A. Osinsky, V. Fuflyigin, and L. D. Zhu, “Infrared spectroscopy of ZnSiN2 single-crystalline films on r-sapphire”, Appl. Phys. Lett., 76(18): 2517, 2000

[29] T.R.Paudel, “Structure, Phonons and related Properties in Zn-IV-N2 (IV=Si,Ge,Sn), ScN and Rare-Earth Nitrides”, PhD thesis, Case Western Reserve University, 2008

[30] P.C.Quayle, K. L. He, J. Shan, and K.Kash, “Synthesis, lattice structure, and bandgap of ZnSnN2”, MRS Communications, 3:135-138, 2013.

[31] W. Walukiewicz, J. W. Ager, K. M. Yu, Z. Liliental-Weber, J. Wu, S. X. Li, R. E. Jones, and J. D. Denlinger, “Structure and electronic properties of InN and In-rich group III-nitride alloys”. J. Phys. D: Appl. Phys., 39, R83, 2006

[32] B. D. Cullity, “Elements of x-ray diffraction”, second edition, Addison-Wesley Publishing Company, Inc., 1978.

[33] N. K. Jiang, “Reactive Sputtering Deposition and Characterization of Zinc Nitride and Oxy-Nitride Films for Electronic and Photovoltaic Applications”, PhD thesis, The University of Toledo, 2013.

[34] U. K. MISHRA, and J. SINGH, “SEMICONDUCTOR DEVICE PHYSICS AND DESIGN”, Springer, The Netherlands, 2008.

[35] Fioretti, A. N., Toberer, E. S., Zakutayev, I. A., & Tamboli, A. C. (2015). Effects of Low Temperature Annealing on the Transport Properties of Zinc Tin Nitride, XX(X), 1–5.

[36] P. C. Quayle, K. He, J. Shan, and K. Kash, “Synthesis, lattice structure, and band gap of ZnSnN2,” MRS Communications, vol. 3, pp. 135–138, 2013.

[37] S.M. Sze and K.K. Ng. *Physics of semiconductor devices*. John Wiley & Sons, 2006.

[38] Fioretti, A. N., Zakutayev, A., Moutinho, H., Melamed, C., Toberer, E. S., & Tamboli, A. C. (2015). Materials Chemistry C.

[39] A. Punya, T. R. Paudel and W. R. L. Lambrecht, Physica Status Solidi C, 2011, 8, 2492-2499.

[40] N. Feldberg, J. D. Aldous, W. M. Linhart, L. J. Phillips, K. Durose, P. A. Stampe, R. J. Kennedy, D. O. Scanlon, G. Vardar, R. L. F. III, T. Y. Jen, R. S. Goldman, T. D. Veal and S. M. Durbin, Applied Physics Letters, 2013, 103, 042109.

[41] Shing, A. M., Coronel, N. C., Lewis, N. S., Atwater, H. A., Shing, A. M., Coronel, N. C; Atwater, H. A. (2016). Semiconducting ZnSnxGe1-xN2 alloys prepared by reactive radio-frequency sputtering Semiconducting $ZnSn_xGe_{1-x}N_2$ alloys prepared by reactive radio-frequency sputtering, 076104(2015).

[42] Lahourcade, L., Coronel, N. C., Delaney, K. T., Shukla, S. K., Spaldin, N. A., & Atwater, H. A. (2013). Structural and Optoelectronic Characterization of RF Sputtered ZnSnN 2, 1–5.

[43] Chen, S., Narang, P., Atwater, H. A., & Wang, L. (2014). Phase Stability and Defect Physics of a Ternary $ZnSnN_2$ Semiconductor : First Principles Insights, 311–315.